

Demonstration of a heterogeneously integrated III-V/SOI single wavelength tunable laser

Shahram Keyvaninia,^{1,2,*} Gunther Roelkens,^{1,2} Dries Van Thourhout,^{1,2}
Christophe Jany,³ Marco Lamponi,³ Alban Le Liepvre,³ Francois Lelarge,³
Dalila Make,³ Guang-Hua Duan,³ Damien Bordel,⁴ and Jean-Marc Fedeli⁴

¹Photonics Research Group, Ghent University-imec, Sint-Pietersnieuwstraat 41, B-9000 Ghent, Belgium

²Center for Nano- and Biophotonics (NB-Photonics), Ghent University, Ghent, Belgium

³III-V lab, III-V Lab, a joint lab of 'Alcatel-Lucent Bell Labs France', 'Thales Research and Technology' and 'CEA Leti', Campus Polytechnique, 1, Avenue A. Fresnel, 91767 Palaiseau cedex, France

⁴CEA- LETI, Minatec 17 Rue des Martyrs Grenoble France

*shahram.keyvaninia@intec.ugent.be

Abstract: A heterogeneously integrated III-V-on-silicon laser is reported, integrating a III-V gain section, a silicon ring resonator for wavelength selection and two silicon Bragg grating reflectors as back and front mirrors. Single wavelength operation with a side mode suppression ratio higher than 45 dB is obtained. An output power up to 10 mW at 20 °C and a thermo-optic wavelength tuning range of 8 nm are achieved. The laser linewidth is found to be 1.7 MHz.

©2013 Optical Society of America

OCIS codes: (250.0250) Optoelectronics; (250.5300) Photonic integrated circuits; (250.5960) Semiconductor lasers.

References and links

1. S. Selvaraja, W. Bogaerts, P. Dumon, D. Van Thourhout, and R. Baets, "Sub-nanometer linewidth uniformity in silicon nano-phonic waveguide devices using CMOS fabrication technology," *IEEE J. Sel. Top. Quantum Electron.* **16**(1), 316–324 (2010).
2. S. Keyvaninia, M. Muneeb, S. Stanković, P. J. Van Veldhoven, D. Van Thourhout, and G. Roelkens, "Ultra-thin DVS-BCB adhesive bonding of III-V wafers, dies and multiple dies to a patterned silicon-on-insulator substrate," *Opt. Mater. Express* **3**(1), 35–46 (2013).
3. D. Liang, A. W. Fang, H. Park, T. E. Reynolds, K. Warner, D. C. Oakley, and J. E. Bowers, "Low-Temperature, Strong SiO₂-SiO₂ Covalent Wafer Bonding for III-V Compound Semiconductors-to-Silicon Photonic Integrated Circuits," *J. Electron. Mater.* **37**(10), 1552–1559 (2008).
4. J.-M. Fedeli and B. Ben Bakir, "InP on SOI devices for optical communication and optical network on chip," in *Proceedings of SPIE Photonic West Conference, 7942 Optoelectronic Integrated Circuits XIII* (San Francisco, California, USA, 2011).
5. H. Park, A. W. Fang, O. Cohen, R. Jones, M. J. Paniccia, and J. E. Bowers, "An electrically pumped AlGaInAs-silicon evanescent amplifier," *IEEE Photon. Technol. Lett.* **19**(4), 230–232 (2007).
6. S. Keyvaninia, G. Roelkens, D. Van Thourhout, G. H. Duan, M. Lamponi, F. Lelarge, J.-M. Fedeli, S. Messaoudene, E. J. Geluk, and B. Smalbrugge, "A highly efficient electrically pumped optical amplifier integrated on a SOI waveguide circuit," in *Proceedings of IEEE Group IV Photonics Conference* (San Diego, United States, 2012), 222–224.
7. S. Keyvaninia, G. Roelkens, and D. Van Thourhout, "Engineering the heterogeneously integrated III-V/SOI tunable laser," in *Proceedings of 14th Ann. Symp. IEEE Photonics Benelux Chapter* (Belgium, 2009), 141–144.
8. M. Lamponi, S. Keyvaninia, C. Jany, F. Poingt, F. Lelarge, G. de Valicourt, G. Roelkens, D. Van Thourhout, S. Messaoudene, J.-M. Fedeli, and G. H. Duan, "Low-threshold heterogeneously integrated InP/SOI lasers with a double adiabatic taper coupler," *IEEE Photon. Technol. Lett.* **24**(1), 76–78 (2012).
9. A. W. Fang, H. Park, O. Cohen, R. Jones, M. J. Paniccia, and J. E. Bowers, "Electrically pumped hybrid AlGaInAs-silicon evanescent laser," *Opt. Express* **14**(20), 9203–9210 (2006).
10. S. Stanković, R. Jones, M. Sysak, J. Heck, G. Roelkens, and D. Van Thourhout, "1310 nm hybrid III-V/Si Fabry-Perot laser based on adhesive bonding," *IEEE Photon. Technol. Lett.* **23**(23), 1781–1783 (2011).
11. G. Roelkens, L. Liu, D. Liang, R. Jones, A. Fang, B. Koch, and J. Bowers, "III-V/silicon photonics for on-chip and inter-chip optical interconnects," *Laser Photon. Rev.* **4**(6), 751–779 (2010).
12. T. Maruyama, T. Okumura, S. Sakamoto, K. Miura, Y. Nishimoto, and S. Arai, "GaInAsP/InP membrane BH-DFB lasers directly bonded on SOI substrate," *Opt. Express* **14**(18), 8184–8188 (2006).

13. A. W. Fang, E. Lively, Y. H. Kuo, D. Liang, and J. E. Bowers, "A distributed feedback silicon evanescent laser," *Opt. Express* **16**(7), 4413–4419 (2008).
14. A. W. Fang, B. R. Koch, R. Jones, E. Lively, D. Liang, Y.-H. Kuo, and J. E. Bowers, "A distributed Bragg reflector silicon evanescent laser," *IEEE Photon. Technol. Lett.* **20**(20), 1667–1669 (2008).
15. D. Van Thourhout, L. Zhang, W. Yang, B. I. Miller, N. J. Sauer, and C. R. Doerr, "Compact digitally tunable laser," *IEEE Photon. Technol. Lett.* **15**(2), 182–184 (2003).
16. J. Buus, M.-C. Amamm, and D. Blumenthal, *Tunable Laser Diodes and Related Optical Sources*, 2nd ed. (Wiley-IEEE Press, 2005).
17. M. J. R. Heck, A. La Porta, X. J. M. Leijtens, L. M. Augustin, T. de Vries, B. Smalbrugge, Y.-S. Oei, R. Nötzel, R. Gaudino, D. J. Robbins, and M. K. Smit, "Monolithic AWG-based discretely tunable laser diode with nanosecond switching speed," *IEEE Photon. Technol. Lett.* **21**(13), 905–907 (2009).
18. B. Liu, A. Shakouri, and J. E. Bowers, "Wide tunable double ring resonator coupled lasers," *IEEE Photon. Technol. Lett.* **14**(5), 600–602 (2002).
20. T. Segawa, S. Matsuo, T. Kakitsuka, T. Sato, Y. Kondo, and R. Takahashi, "Semiconductor double-ring-resonator-coupled tunable laser for wavelength routing," *IEEE J. Quantum Electron.* **45**(7), 892–899 (2009).
19. T. Chu, N. Fujioka, and M. Ishizaka, "Compact, lower-power-consumption wavelength tunable laser fabricated with silicon photonic-wire waveguide micro-ring resonators," *Opt. Express* **17**(16), 14063–14068 (2009).
21. A. Le Liepvre, C. Jany, A. Accard, M. Lamponi, F. Poingt, D. Make, F. Lelarge, J.-M. Fedeli, S. Messaoudene, D. Bordel, and G.-H. Duan, "Widely wavelength tunable hybrid III-V/silicon laser with 45 nm tuning range fabricated using a wafer bonding technique," in *Proceedings of IEEE Group IV Photonics Conference* (San Diego, United States, 2012), 54–56.
22. "CAMFR," <http://camfr.sourceforge.net>
23. D. Derrickson, *Fiber Optic Test and Measurement* (Prentice Hall, 1998), p. 185.
24. G. H. Duan, C. Jany, A. Le Liepvre, J. G. Provost, D. Make, F. Lelarge, M. Lamponi, F. Poingt, J.-M. Fedeli, S. Messaoudene, D. Bordel, S. Brisson, S. Keyvaninia, G. Roelkens, D. Van Thourhout, D. J. Thomson, F. Y. Gardes, and G. T. Reed, "10 Gb/s integrated tunable hybrid III-V/si laser and silicon mach-zehnder modulator," in *Proceedings of European Conference and Exhibition on Optical Communication ECEOC* (Amsterdam, 2012).

1. Introduction

Silicon-On-Insulator (SOI) is gaining interest as a novel platform for integrated optical circuits, since its large refractive index contrast allows for ultra-compact devices. The interest in this technology stems however mostly from the expectation that the maturity and low cost of CMOS-technology can be applied for advanced photonics products [1]. The heterogeneous integration of III-V semiconductors on silicon using a wafer bonding technique is currently the most relevant solution for the fabrication of laser sources on silicon. Such integration allows creating integrated optical devices, which take the best of both worlds: III-V semiconductors for efficient light emission and amplification and silicon for its low loss and high index contrast waveguiding. In order to densely integrate the III-V semiconductor with the silicon waveguide circuits, mainly molecular wafer bonding and DVS-BCB adhesive bonding techniques [2–4] are used and are actively reported in state-of-the-art hybrid amplifiers [5,6] and lasers [7–11]. In these approaches, unstructured InP-based dies are bonded, epitaxial layers down, on an SOI waveguide circuit wafer, after which the InP growth substrate is removed and the III-V epitaxial film is processed. The design space for hybrid InP/SOI devices is large and in particular the coupling between the optical mode in the top active III-V waveguide and that in the bottom passive SOI waveguide plays an important role. In literature, two main solutions are reported. In the first approach, based on evanescent coupling, the bulk of the optical mode (~70%) in the III-V/silicon amplifier waveguide is confined within the Si waveguide [5,9,10]. Typically, the silicon waveguide thickness is larger than 500 nm and the III-V effective waveguide width is large (>4 μm). In the second type of devices, the optical mode is mostly confined in the III-V material. In this case, coupling between the III-V and silicon waveguide is realized by adiabatically tapering the silicon and III-V waveguide [6–8]. This requires that the thickness of the bonding layer is thin enough (<100 nm) to have high coupling efficiency.

Several applications require single wavelength and wavelength tunable lasers. Several single wavelength lasers on a III-V/silicon photonics platform have been demonstrated, both based on distributed feedback (DFB) and distributed Bragg reflector (DBR) geometries [11–14]. The demonstrated heterogeneous III-V/SOI DBR lasers consist of two passive Bragg

reflector mirrors etched on silicon waveguides. Single mode operation was also demonstrated, with a lasing threshold of 65 mA and a maximum front mirror output power of 11 mW [14]. In the heterogeneously integrated DFB laser demonstrations, the optical mode is mainly guided by a silicon waveguide and the tail of the optical mode overlaps with the multiple quantum well gain region. A threshold current around 25 mA and slope efficiency around 0.05 mW/mA was demonstrated [13]. Wavelength tunable semiconductor lasers are now commonly used to replace conventional DFB lasers. This avoids the need for an extra set of DFB-laser-installed interface boards as a backup for device failure, and they significantly reduce the cost of the selection of wavelength-suitable laser devices and the inventory of laser devices for industrial production. There are several approaches for the design of integrated tunable lasers: sampled grating DBR (SGDBR), digitally tuned DBR lasers, etc., mainly developed on InP substrates [15–17]. Recently, tunable lasers integrating extra-cavity or intra-cavity ring resonators (RRs) have been demonstrated on InP [18,19], or by butt-coupling an already fabricated reflective semiconductor optical amplifier to an external ring resonator filter fabricated on SOI [20]. However, InP-based solutions still suffer from high losses in passive parts and yield issues, while the butt-coupling solution requires high precision mechanical positioning, which is costly and not suitable for dense photonic integration. Moreover, to achieve single mode lasing ring filters with a large free spectral range (FSR) are required, which can be easily realized on the silicon photonics platform due to the high refractive index contrast, compared to the low index contrast available on InP-based integrated circuits.

This paper reports on a detailed study of a new heterogeneously integrated tunable laser fabricated using a wafer bonding technique, presenting several new features: narrow III–V waveguides in the range from 2 to 3 μm , thin silicon waveguide thickness (400 nm/220 nm) and an adiabatic taper in both the III–V and silicon waveguide. A single ring resonator is integrated inside the laser cavity allowing very simple wavelength tuning. Such a combination allows us to demonstrate a single wavelength laser with 45mA threshold at 20°C, more than 8 nm tuning range and a side mode suppression ratio (SMSR) larger than 40 dB over the tuning range. The maximum power coupled to a lensed fiber is 0 dBm at 20 °C, while the total output power from the laser itself is around 10 dBm. The laser linewidth is measured to be 1.7 MHz. Based on this technology recently a widely tunable laser based on the Vernier effect in a double ring configuration was also demonstrated [21]. The paper is organized as follows: Section 2 is devoted to present the design and characterization of the passive and active section of the tunable laser. Section 3 focuses on the fabrication process. In Section 4 the laser characteristics are reported.

2. Device structure

2.1. Laser cavity design

In order to reach single longitudinal mode lasing, at least one of the reflectors has to provide a narrow band reflection, with a bandwidth on the order of the longitudinal mode spacing of the laser cavity. Also, the FSR of that filter is preferably larger than the gain bandwidth of the amplifier section, to provide a predictable laser wavelength. In this work, the wavelength feedback was realized using a broadband, high reflectivity DBR mirror at one end of the laser cavity and a combination of a ring resonator and partially reflecting DBR on the other side of the laser cavity, as schematically illustrated in Fig. 1(a). The ring resonator structure that is used has a large FSR (see section 2.3) such that there is only one resonance within the 1 dB reflection bandwidth of the DBR grating as schematically illustrated in Fig. 1(b). As illustrated in Fig. 1(a), the InP-based amplifier waveguide is coupled to the silicon waveguide circuit using an adiabatic mode converter. A metallic heater is implemented on top of the ring resonator to allow thermal tuning of the resonance wavelength.

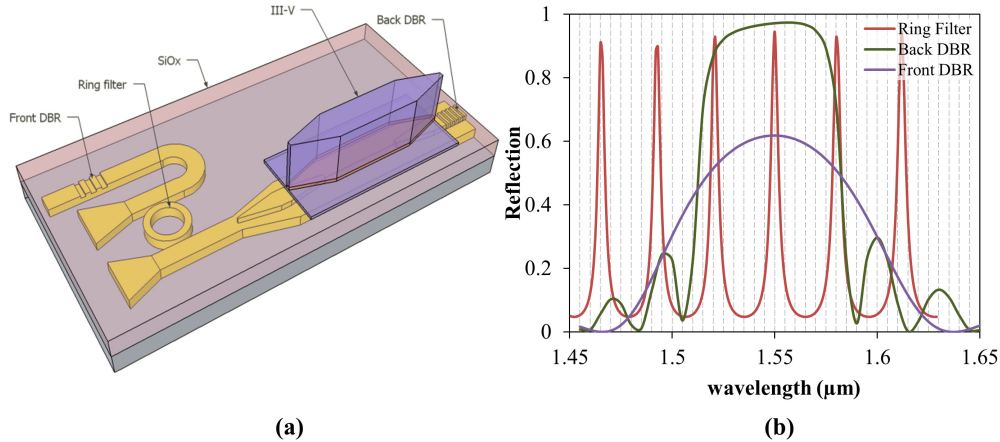


Fig. 1. (a) Schematic view of the single wavelength microring-based laser structure; (b) Reflection characteristic of the ring resonator (red), and DBR grating (blue/green) combination; and the longitudinal mode spacing is added (dashed lines) as a reference.

2.2. DBR design

The silicon waveguide structures were fabricated in a CMOS pilot-line at CEA-LETI, on an SOI wafer using a 400 nm silicon device layer thickness. The etch modules available in this process were limited to 180 nm, 50 nm and 220 nm. To achieve narrow band Bragg reflectors especially with the top corrugation DBR envisioned in this work, these gratings were implemented in 220 nm high, vertically single mode, waveguides with 50 nm etch depth. These Bragg reflectors were simulated using the open-source full-vectorial eigenmode solver CAMFR [22] to calculate the first-order to first-order mode reflection of the structure as a function of wavelength.

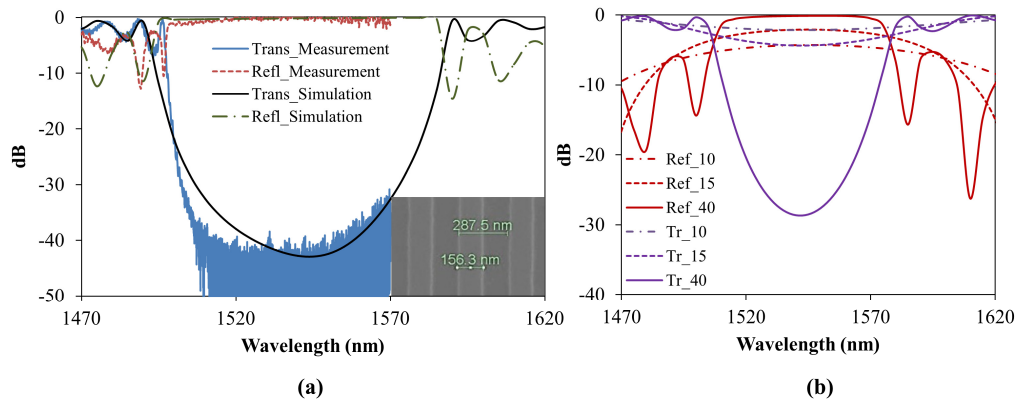


Fig. 2. (a) Simulation of a Bragg reflector and experimental measurements for structures using a 70 nm grating etch depth with a grating period of 290 nm and 50% duty cycle (40 periods); (b) Simulation of the grating transmission ($Tr_{_}$) and reflection ($Ref_{_}$) for 10, 15, and 40 periods; the Bragg reflector used in this work has a 50 nm grating etch depth with a grating period of 280 nm and 50% duty cycle.

In order to verify the simulation results, devices from a separate run, fabricated using the ePIXfab multi-project wafer service, using a 70 nm etch module on a 220 nm thick waveguides were fabricated. The measurement and simulation results are shown in Fig. 2(a). The duty cycle of the grating was fixed at 50%. The grating period was fixed at 290 nm for achieving maximal reflection around 1550 nm, and 40 grating periods were implemented.

Clearly a good correspondence between simulation and measurement was achieved, allowing a well-supported design of the actual 50 nm etch depth DBR gratings for the laser structure. For this design the grating period changed to 280 nm to achieve maximal reflection around 1550 nm. Simulation results for the reflection and transmission spectrum for 10, 15 and 40 periods are shown in Fig. 2(b).

2.3. Ring filter design

As was shown in Fig. 1(b), to achieve single mode laser operation, the FSR of the resonator should be larger than the reflection bandwidth of the DBR gratings. A scanning electron microscope image of the racetrack resonator structure fabricated in the 220 nm silicon device layer used in this work is shown in the inset of Fig. 3. The bus and ring waveguide width was 500 nm, the radius was 3.1 μm , while the coupling section was 2.8 μm long, with a gap of 180 nm between the bus and racetrack waveguide. A FSR of 25 nm was targeted in this work. The ring resonators used in the laser cavity were characterized by injecting light into the fabricated device structure, using the III-V gain section under reverse bias to operate as a photodetector. The measurements were carried out by cleaving off the front DBR reflector in order to assess the ring resonator characteristics over a broad wavelength range. The measurements are presented in Fig. 3, illustrating a FSR of 25 nm and a quality factor of 1500.

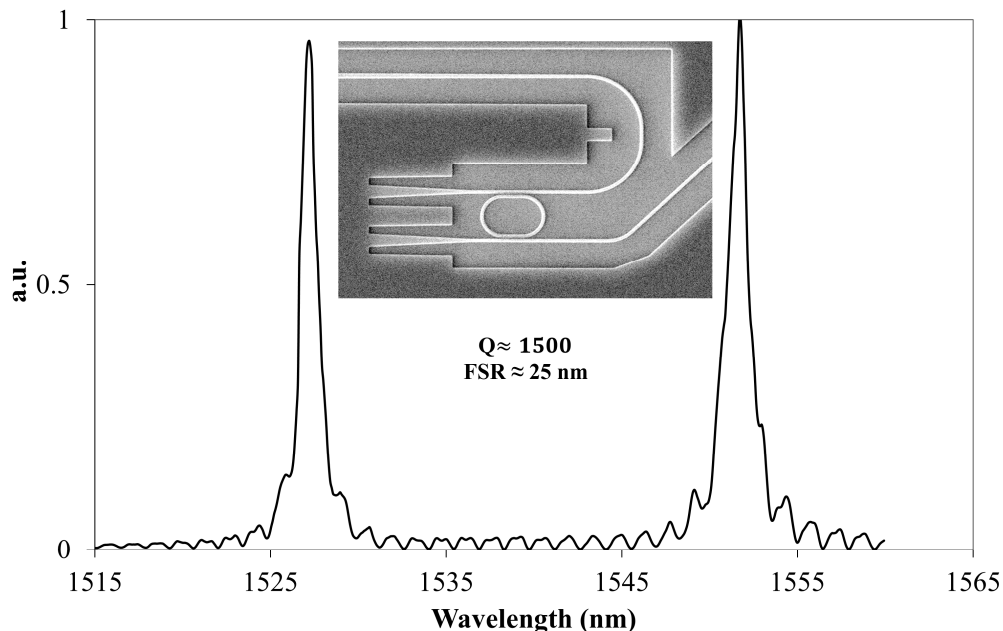


Fig. 3. Characterization of the ring resonator structure by using the III-V gain region under reverse bias; the inset shows a scanning electron microscope image of the fabricated structure.

2.4. III-V waveguide and coupling design

A bonded structure of an InGaAsP quantum well p-i-n diode layer stack and a silicon waveguide forms the heterogeneously integrated amplifier section. The III-V region consists of a p-InGaAs contact layer, a p-InP cladding layer (1.5 μm thick), six InGaAsP quantum wells (6 nm) surrounded by two InGaAsP separate confinement heterostructure (SCH) layers (100 nm thick; bandgap wavelength 1.17 μm), and an n-type InP layer (200 nm). The SOI substrate (200 mm wafer manufactured by SOITEC) is composed of a 400 nm mono-

crystalline silicon layer on top of a 2 μm thick buried oxide layer on a silicon substrate. The silicon rib waveguides in the laser gain region have a height of 400 nm and an etch depth of 180 nm. The III-V membrane layer is bonded onto the silicon waveguide circuit using a molecular wafer bonding approach [4]. The design of the gain section in the laser is schematically illustrated in Fig. 4. The structure can be divided into three parts. In the center of the device there is a III-V waveguide that provides optical gain, by confining the optical mode in the III-V waveguide layer. This III-V waveguide is 2 or 3 μm wide, depending on the design, and is etched through the active layer to be able to access the n-type contact. At both sides of this section there is an adiabatic inverted taper coupler for high efficiency and large optical bandwidth coupling between the III-V membrane layer and the silicon waveguide layer. In the adiabatic taper section, the width of the III-V mesa is tapered from 900 nm to 300 nm, while the silicon rib waveguide underneath is tapered from 300 nm to 1 μm over a length of 150 μm (Taper II). The III-V mesa width is tapered more abruptly from 2 μm (3 μm) to 900 nm over 30 μm (50 μm) (Taper I). After the coupling region the light is guided by the 400 nm silicon rib waveguide, which is transferred to the 220 nm silicon device layer using a low-loss 400 nm to 220 nm waveguide transition (taper length: 30 μm , taper tip width: 100 nm).

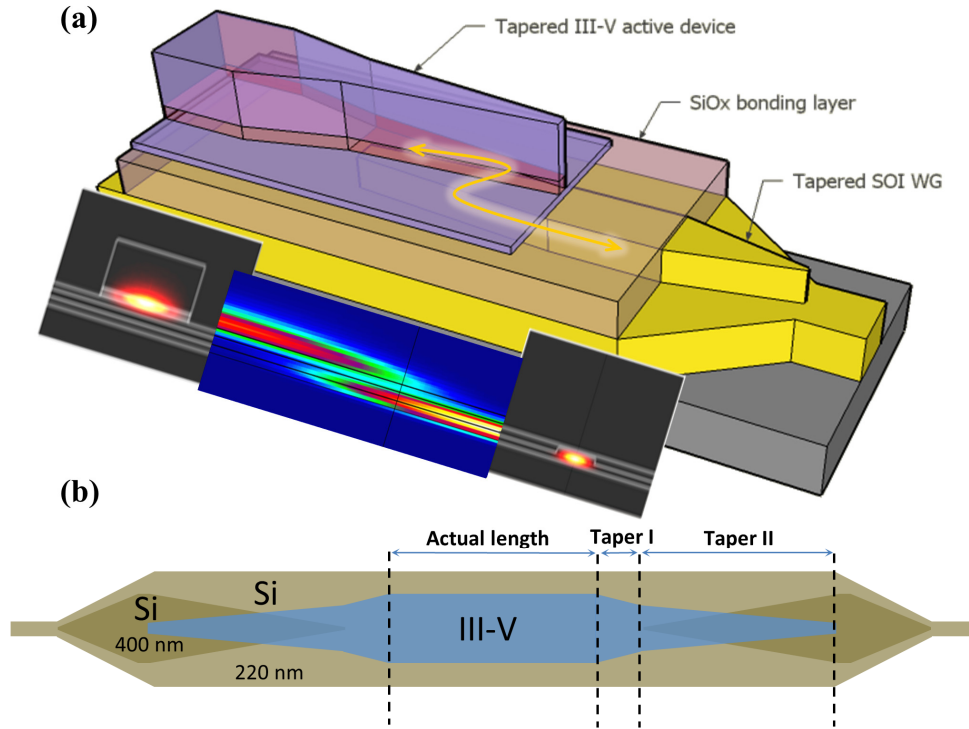


Fig. 4. (a) Three-dimensional view of the coupling structure in the gain section with representative mode profiles in two cross-sections; (b) detailed top view of the gain structure.

3. Device fabrication

The fabrication process begins with the processing of the SOI wafer incorporating a 400 nm thick silicon waveguide layer in a CMOS pilot line. The first step is the lithography and etching of 180 nm silicon, allowing the realization of 400 nm rib waveguides for the coupling between the III-V gain section and silicon waveguides. The second step is the lithography and etching of a 50 nm silicon layer, necessary for the realization of Bragg gratings and fiber-to-chip grating couplers in the 220 nm device layer. Afterwards, the silicon strip waveguides are

etched. Next, a SiO₂ cladding layer was deposited and the wafer was planarized using chemical mechanical polishing (CMP). Afterwards, a 2-inch InP-based epitaxial wafer was bonded onto the processed SOI wafer, using molecular bonding [4]. After removal of the InP substrate using wet chemical etching, the InP membrane gain section can be processed. The first step of the processing is to define the III-V waveguide including the taper for the coupling with a silicon waveguide. The definition of the III-V waveguide was performed using deep UV lithography in order to get a fine taper tip (300 nm) and an alignment with the underlying silicon waveguide layer better than ± 150 nm. Once this step is completed, the large 8" SOI wafer is cut into 3" wafers to be processed in a III-V cleanroom. Figure 5(a) shows a picture of a completely processed 3" hybrid III-V/SOI wafer. The details of the III-V processing sequence are described in [8]. Finally, a NiCr metal layer is deposited on the top of the ring resonators for thermal tuning of the ring resonator devices. A microscope image of the fabricated laser structures is shown in Fig. 5(b).

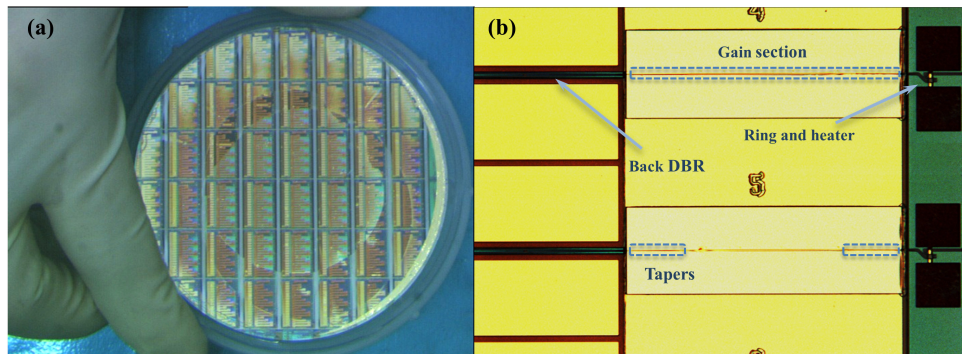


Fig. 5. (a) Picture of a completely processed III-V/SOI wafer; (b) microscope picture of the fabricated tunable lasers, showing the ring resonator section with integrated heater, the III-V gain section (after metallization) and the passive silicon output waveguide.

4. Measurement results

To characterize the lasers, the silicon chip is cleaved either after or before the front DBR. In the first configuration, the reflectivity of the front DBR (with 12 periods) was relatively high ($\sim 50\%$) which causes lower threshold current but also lower output power. Continuous wave (CW) lasing with a 38 mA threshold current (for a 500 μm long and 2 μm wide gain section) is achieved with this configuration at 20°C. Figure 6(a) shows an example of the L-I curve of a ring-resonator-based laser under CW operation regime at different temperatures. The maximum output power is around 4 mW at 20°C, and the output power is higher than 0.8 mW at 60°C.

Spectral measurements were performed using a single-mode lensed fiber connected to an optical spectrum analyzer with a resolution bandwidth of 0.1 nm. Figure 6(b) clearly shows single mode operation with 50 dB SMSR. Such a large SMSR is attributed to the narrow bandwidth of the racetrack resonator structure. The background spectrum is due to spontaneous emission (filtered by the ring resonator) from the gain section coupled to the silicon output waveguide.

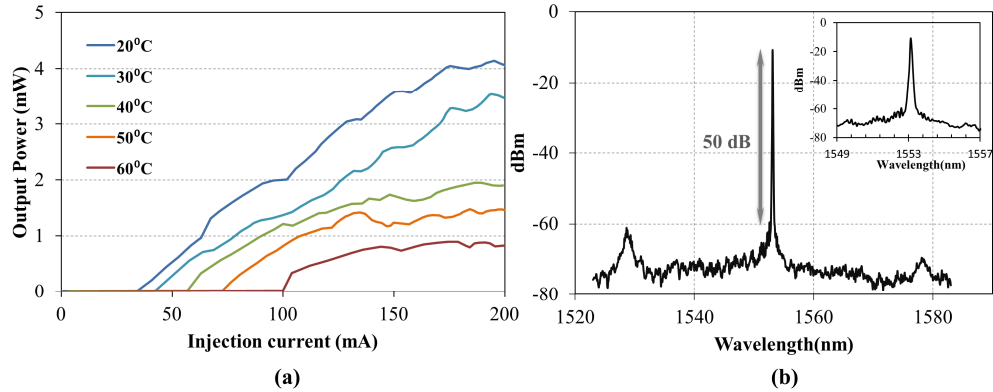


Fig. 6. (a) the L-I curve of the hybrid ring-resonator-based laser with two DBRs in CW regime as a function of temperature; (b) measured laser spectrum showing more than 50 dB side mode suppression ratio (at 20°C for 80 mA current injection).

By cleaving the laser structure before the front DBR, the resulting output facet reflectivity is around 30%. Compared to the previous case this configuration gives a higher output power as well as higher threshold currents. Continuous wave output power-gain section bias current-gain section voltage (LIV) results are shown in Fig. 7(a) for 20°C continuous wave operation, showing up to 10 mW output power collected by a photodiode located in front of the cleaved facet (for a 500 μm long and 2 μm wide gain section).

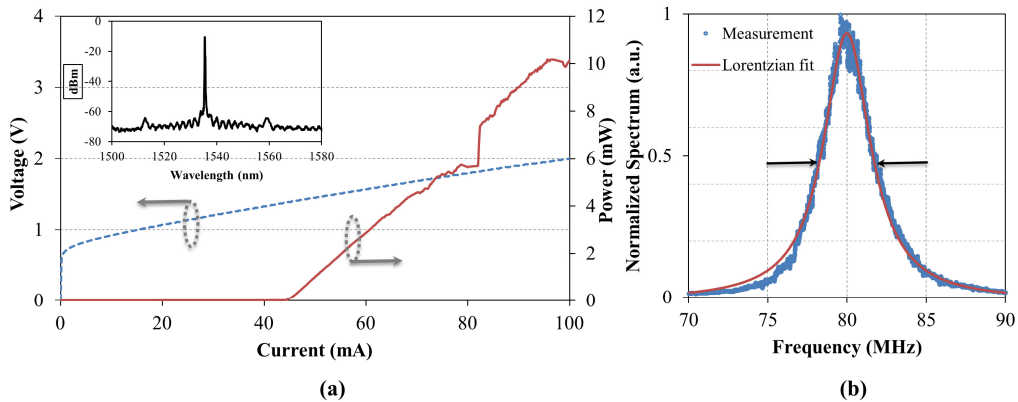


Fig. 7. (a) The L-I-V curve for a hybrid ring-resonator-based laser with a back DBR and a cleaved front facet at 20°C. The inset shows the lasing spectrum for this device configuration. (b) Delayed-self heterodyne line width trace at 20°C and laser injection current of 80 mA and the Lorentzian fit illustrating 1.7 MHz laser line width.

The laser line width was measured using a delayed-self heterodyne method [23], using an 80 MHz modulation and 22.5 km of single mode fiber. The line shape of the beat signal is measured on an RF spectrum analyzer with a 10 kHz resolution bandwidth, which is illustrated in Fig. 7(b), showing the measurement data and the Lorentzian fit. The Lorentzian fit has a 3 dB bandwidth of 3.4 MHz, which corresponds to a 1.7 MHz FWHM laser linewidth for 80 mA current injection.

A NiCr heater (20 Ohm) deposited above the ring resonator allows to thermally tune the resonance frequency of the ring resonator. As a result, by tuning the ring resonator, the lasing cavity mode will jump to the one with the lowest threshold and hence a tunable laser can be realized. Figure 8 shows an example of the super-imposed optical spectra with several values of the heating power. One can observe from this figure that we achieve a wavelength tuning

range of 8 nm. Over the full range single mode operation with a SMSR larger than 40 dB is achieved. The wavelength tuning is not continuous due to longitudinal mode hopping. This phenomenon is typical for this kind of cavity where no phase section is implemented. The thermal tuning efficiency is 3.2 nm/10 mW. Looking carefully at the tuning curve of the laser shown in Fig. 8(b), it can be observed that the mode can jump from mode N to $N + 1$ or even jump from N to $N + 2$ at some heater power levels, as the wavelength hops correspond to a single or double free spectral range (FSR is 250 pm) of the laser cavity.

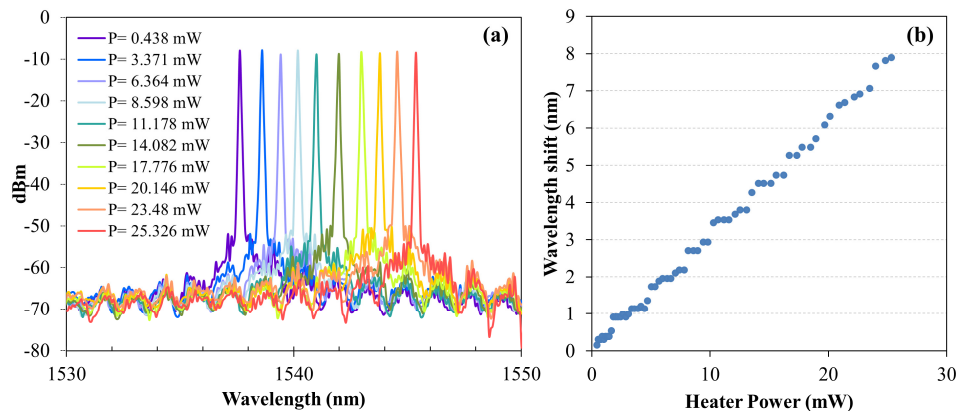


Fig. 8. (a) Super-imposed laser spectra for several values of the heating power (b) laser wavelength as a function of the power dissipated in the heater, at 20°C and a laser injection current of 80 mA.

5. Conclusions

In this paper we demonstrate the use of the III-V on silicon platform for the realization of tunable single wavelength lasers. An 8 nm tuning range is realized, with optical output powers in the range of 10 mW at room temperature. We recently demonstrated that such a laser can be also be integrated with high speed silicon modulators [24]. Such a laser structure can become an important device for future telecommunication and data communication systems. It is also of great interest in the field of spectroscopic sensing when widely tunable light sources without moving parts and with high optical output power are needed.

Acknowledgments

This work was supported by the FP7-IP-HELIOS project. The authors would like to thank Lemos Alvares Dos Santos and Saeed Tahvili from Eindhoven University of Technology for the assistance with the linewidth measurements.